Journal of Photochemistry & Photobiology, B: Biology 231 (2022) 112449

Contents lists available at ScienceDirect

Journal of Photochemistry & Photobiology, B: Biology

journal homepage: www.elsevier.com/locate/jphotobiol

Photosensitization of pancreatic cancer cells by cationic alkyl-porphyrins in free form or engrafted into POPC liposomes: The relationship between delivery mode and mechanism of cell death

Eros Di Giorgio [a,1], Annalisa Ferino [a,1], Himanshi Choudhary [a], Phillip M.G. Löffler [b], Francesca D'Este [a], Valentina Rapozzi [a], Alexander Tikhomirov [c], Andrey Shchekotikhin [c], Stefan Vogel [b], Luigi E. Xodo [a,*]

[a] Department of Medicine, Laboratory of Biochemistry, University of Udine, P.le Kolbe 4, 33100 Udine, Italy
[b] Department of Physics, Chemistry and Pharmacy, University of Southern Denmark, Odense, Denmark
[c] Gause Institute of New Antibiotics, B. Pirogovskaya 11, 119021 Moscow, Russia

ARTICLE INFO

Keywords:
Alkyl-porphyrins
POPC liposomes
Photodynamic therapy
KRAS
GXP4
Apoptosis
Ferroptosis

ABSTRACT

Cationic porphyrins bearing an alkyl side chain of 14 (**2b**) or 18 (**2d**) carbons dramatically inhibit proliferation of pancreatic cancer cells following treatment with light. We have compared two different ways of delivering porphyrin **2d**: either in free form or engrafted into palmitoyl-2-oleoyl-sn-glycero-3-phosphocholine liposomes (L-**2d**). Cell cytometry shows that while free **2d** is taken up by pancreatic cancer cells by active (endocytosis) and passive (membrane fusion) transports, L-**2d** is internalized solely by endocytosis. Confocal microscopy showed that free **2d** co-localizes with the cell membrane and lysosomes, whereas L-**2d** partly co-localizes with lysosomes and ER. It is found that free **2d** inhibits the *KRAS*-Nrf2-GPX4 axis and strongly triggers lipid peroxidation, resulting in cell death by ferroptosis. By contrast, L-**2d** does not affect the *KRAS*-Nrf2-GPX4 axis and activates cell death mainly through apoptosis. Overall, our study demonstrates for the first time that cationic alkyl porphyrins, which have a IC_{50} ~ 23 nM, activate a dual mechanism of cell death, ferroptosis and apoptosis, where the predominant form depends on the delivery mode.

1. Introduction

The use of nanoparticles for drug delivery is an important area of investigation in cancer therapy. Among the nanostructures proposed as drug-delivery vehicles, liposomes have drawn the attention of many researches as they are easily prepared and composed by non-toxic naturally occurring phospholipids [1–4]. They consist of a spherical phospholipid bilayer delimiting an aqueous central core space and are employed as nanocarrier for drug delivery in cancer. Due to their unique capacity to entrap both hydrophobic and hydrophilic compounds, liposomes are used to transport into the tissues a wide range of drugs [5]. In fact, lipophilic molecules can be engrafted into the membrane bilayer, whereas hydrophilic compounds can be entrapped in the aqueous central core [1–4]. Liposomes are attractive drug carriers because they are easily suspended in aqueous solution, they are non-immunogenic and biodegradable. They also have a good capacity of self-assembly, they possess a high drug loading [6,7] and the drugs loaded in liposomes exhibit, in general, a low systemic toxicity, and are also protected from degradation and inactivation [8–12].

In our study, as drugs to treat pancreatic cancer cells we used two cationic porphyrins: 5,10,15-tris(1-methylpyridinium-4-yl)-20-(1-tetradecylpyridinium-4-yl)porphyrin, **2b**; 5,10,15-tris(1-methylpyridinium-4-yl)-20-(1-octadecylpyridinium-4-yl)porphyrin, **2d**. These molecules possess four positive charges, making them soluble in water, as well as an alkyl chain of either 14 (**2b**) or 18 (**2d**) carbons (Fig. 1D). They have two interesting properties: they generate reactive oxygen species (ROS)

Abbreviations: PDAC, Pancreatic ductal adenocarcinoma; POPC, Palmitoyl-2-oleoyl-sn-glycero-3-phosphocholine; *KRAS*, Kirsten ras; **2b**, 5,10,15-Tris(1-methylpyridinium-4-yl)-20-(1-tetradecylpyridinium-4-yl)porphyrin; **2d**, 5,10,15-Tris(1-methylpyridinium-4-yl)-20-(1-octadecylpyridinium-4-yl)porphyrin; Nrf2, Nuclear factor erythroid 2-related factor 2; GPX4, Glutathione peroxidase 4; ROS, Reactive oxygene species; FACS, Fluorescence-activated Cell Sorter..

* Corresponding author.
E-mail address: luigi.xodo@uniud.it (L.E. Xodo).

[1] EDG and AF contributed equally to this work.

https://doi.org/10.1016/j.jphotobiol.2022.112449
Received 23 December 2021; Received in revised form 18 April 2022; Accepted 21 April 2022
Available online 25 April 2022

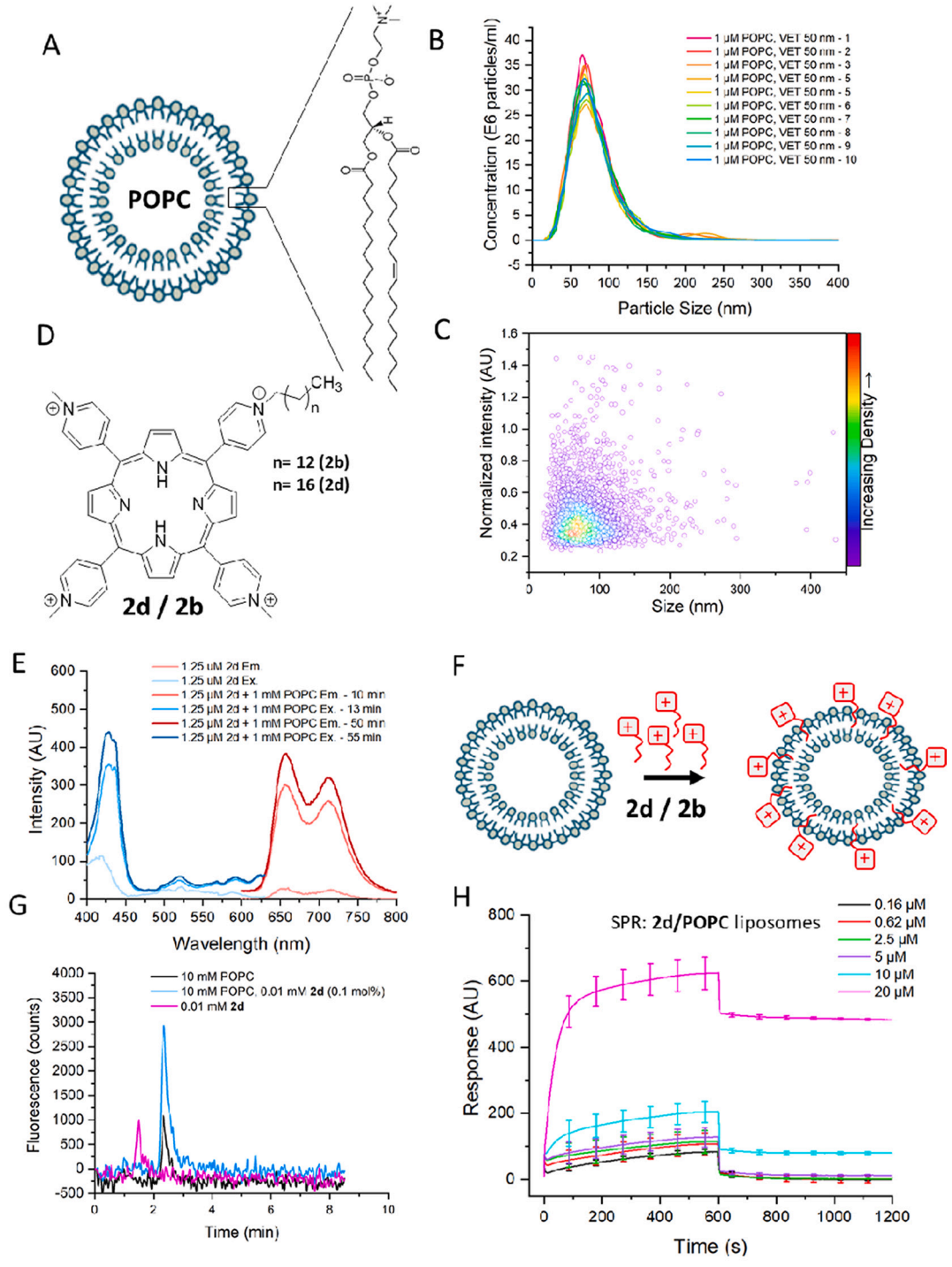

(caption on next page)

Fig. 1. (A) POPC liposomes; (B, C) Nanoparticle Tracking analysis of the liposomes; (D) Stuctures of the cationic porphyrins **2d** and **2b** free or engrafted into POPC liposomes, L-**2d**/L-**2b**; (E) Excitation and emission spectra of **2d** in PBS; (F) Liposome loading with alkyl-porphyrins **2b**/**2d**; (G) Size-exclusion HPLC chromatograms for **2d** and L-**2d**. Fluorescence signal of liposomes loaded with 0.1 mol% **2d** (light blue), native liposomes (visible due to light scattering, black), and porphyrin alone (10 μM, pink); (H) Surface plasmon resonance sensograms showing the binding of **2d** to POPC liposomes immobilized on the sensor chip surface; (I) ROS production in Panc-1 and BxPC-3 cancer cells by porphyrins **2b** and **2d** delivered as free molecules or engrafted into POPC liposomes. L = POPC liposomes. NT = nontreated, illuminated cells. Statistical significance respect to untreated cells (NT): $P \leq 0.05$ (*), 0.01 (**), 0.001 (***). Data relative to: Panc-1/**2d** are the average of 3 independent experiments in duplicate; BxPC3/**2d** and Panc-1/**2b** one experiment in duplicate. (For interpretation of the references to colour in this figure legend, the reader is referred to the web version of this article.)

and singlet oxygen ($^1O_2$) upon illumination with visible light; they tightly bind to G-quadruplex (G4) structures located in the promoter and 5′-untranslated mRNA region of the *KRAS* oncogene [13–16]. The *KRAS* gene is mutated in >90% pancreatic tumours where it reprograms the metabolism in order to produce the biomass necessary for proliferation [17,18]. It plays also the critical role of regulating the ROS homeostasis in PDAC cells by controlling Nrf2, a cellular ROS-sensor [19,20].

Contrarily to conventional chemotherapy, the porphyrins are activated only in the irradiated tumor and not in the surrounding tissues, thus giving limited side effects. Drugs delivered with nanoparticles with a diameter size exceeding the renal clearance threshold can extravasate from leaky tumor vessels and accumulate in the tumor [21]. This makes the drugs associated to nanoparticles more tumor specific than free drugs: a behavior called enhanced permeability retention (EPR) effect. Additionally, as ROS and $^1O_2$ do not diffuse very much from the production site [22], free porphyrins may trigger a different cellular effect than liposome-bound porphyrins, depending on their localization within the cells. In our study we have compared the anticancer activity of alkyl-porphyrins **2b** and **2d** delivered in two different ways: as free molecules or engrafted into POPC liposomes. The results show that both free and POPC-bound porphyrins (L-**2b** and L-**2d**) activate, upon illumination with visible light, a strong photodynamic process that dramatically reduces the cell viability in the nanomolar concentration range. Interestingly, the fraction of **2d** binding to the membrane produces lipid ROS, while the fraction of **2d** located in the cytoplasm inhibits the *KRAS*-Nrf2-GPX4 axis, thus activating cell death by ferroptosis. By contrast, L-**2d**, in which the porphyrin is engrafted into the liposomes, acts as a ROS-generating photosensitizer, promoting cell death mainly by apoptosis. In conclusion, our study demonstrates for the first time that cationic alkyl-porphyrins activate a dual mechanism of cell death: ferroptosis and apoptosis. The former mechanism prevails in cells treated with free alkyl porphyrins, while the latter is predominant when the porphyrins are delivered engrafted into POPC liposomes.

2. Materials and Methods

2.1. Cell Culture, Cell Viability and Proliferation Assay

Pancreatic cancer cells, Panc-1, BxPC-3, MIAPaCa-2 cells were mainained in exponential growth in Dulbecco's Modified Eagle's Medium (DMEM) containing 100 U/ml penicillin, 100 mg/ml streptomycin, 20 mM L-glutammine and 10% Fetal Bovine Serum (Euroclone, MI, Italy). Cell viability were measured by seeding 9×10^3 cells/well in 96-well plate and performing the resazurin assay, photoactivating the porphyrin with a metal halogen lamp (irradiance 8 mW/cm^2 for 15 min, light dose 7.2 J/cm^2). Clonogenic assays were carried out on Panc-1 or BxPC3 cells seeded in a medium after being diluted in a way that a single colony could be formed from each well. After 15 days of growth, the colonies of at least 50 cells were counted and the results reported in bar plots. The IC_{50} values, i.e. the concentration of the porphyrin necessary to reduce the metabolic activity by half, was calculated from dose-response curves.

2.2. Liposome Preparation

POPC (1-palmitoyl-2-oleoyl-sn-glycero-3-phosphocholine, ≥ 99%) was bought from Corden Pharma AG (Switzerland), **2b** and **2d** were synthesized as previously described[13] (**Supplementary S1**). The Phosphate Buffered Saline (PBS, pH 7.4, 10 mM $H_2PO_4^-/HPO_4^{2-}$, 137 mM NaCl, 2.7 mM KCl) for chromatography, spectroscopy and biophysical studies was prepared by dissolving a solid PBS mixture (Sigma-Aldrich) in ultrapure water (18.2 MΩcm^{-1}, MilliQ, MerckMillipore). 10 mM POPC was suspended in PBS and extruded 10 times through a 50 nm diameter polycarbonate membrane (Whatman Nucleopore®, GE Healthcare, Chicago, IL, USA), using a Lipex™ Extruder (Northern Lipids, Burnaby, Canada) and 35–40 bar N_2 pressure. Liposome stock solutions were stored at 4 °C. Liposomes were analyzed by Nanoparticle Tracking Analysis (NTA). Measurements were carried out on a NanoSight LM10-HS equipped with an Andor Lucas EMCCD camera, a LM14 temperature controller and a laser diode operated at 404 nm. The stock solution was diluted with a factor of 10^5 using filtered (to 0.1 μm) PBS. More than 9000 individual particle diffusion tracks were recorded (20 °C, 25 fps, camera gain 450, 10 videos of 15 s). The data was analyzed using the NanoSight NTA 2.3 software. Mode diameter 68 ± 1, Average diameter 85 ± 1 nm, SD of distribution 39 ± 1 nm, 1.95×10^{13} particles/ml for 10 mM POPC). To engraft the alkyl porphyrins to the liposome surface we mixed in phosphate buffer the liposome (16 mM POPC final) and the alkyl porphyrin (20 μM final), the mixture was breafly vortexed and incubated for 1 h at room temperature (phosphate buffer: 10 mM $NaH_2PO_4{\cdot}2H_20$, 5 mM $Na_2HPO_4{\cdot}2H_20$, 140 mM Na^+, pH 7.4). Stock solutions of liposomes functionalized with the porphyrins (L-**2b** and L-**2d**, 0.125 mol%) were stored at 4 °C.

2.3. Surface Plasmon Resonance, Size-Exclusion HPLC and Fluorescence Experiments

A Biacore sensor chip L1 (gold surface engrafted with hydrophobically modified dextran) was used in a Biacore X100 SPR instrument (both GE Healthcare Chicago, IL, USA). The instrument was equilibrated with filtered PBS at 37 °C for 2 h prior to beginning the measurement. During the measurement (37 °C), a suspension of POPC liposomes (0.5 mM lipid concentration,) in PBS was injected as the capture solution (300 s, 6 μl/min), immobilizing intact liposomes on the chip surface.[53,54] After rinsing with PBS at high flow (40 μl/min) and signal equilibration in a flow of PBS (1 μl/min), 0–100 μM solutions of **2b** or **2d** in PBS were injected (contact time 600 s, 1 μl/min) and afterwards their dissociation monitored under a continued slow flow. (600 s, 1 μl/min). The sensorgrams were aligned at the point of the sample injection (both on the time and response axes), and binding and stability values were extracted at 550 s after injection start and end, respectively.

Size-exclusion chromatography and fluorescence experiments are described in **Supplementary S1**.

2.4. FACS, ROS Detection and Annexin-PI Experiments

FACS was performed for uptake studies. Panc-1, BxPC-3 and MIA PaCa-2 cells, plated in a 12-well plate at density of 0.8×10^5 cells/well, were treated only with **2b**/**2d** or with L-**2b**/L-**2d** (1 μM) for 4 h or with 80 μM dynamin inhibitor I, Dynasore (Calbiochem, Merck Millipore, Germany), for 30 min and then with **2b**/**2d** or with L-2b/L-2d (1 μM for 4 h). After incubation, the cells were trypsinized and pelleted. The pellets were resuspended in 500 μl of PBS and immediately analyzed by BD FACSCalibur flow cytometer equipped with a 488 nm argon laser. A minimum of 10^4 cells for each sample were acquired in list mode and

analyzed using Cell Quest software. The cell population was analyzed by FSC and SSC light. The signal was detected by FL3 (680 nm) channel in log scale.

Annexin V–propidium iodide assays were carried out by using the Annexin-V-FLUOS Staining Kit (Roche Diagnostics GmbH, Germany) following the manufacturer instructions. Briefly, Panc-1 (0.9×10^5 cells/well) and BxPC-3 (1.2×10^5 cells/well) cells were seeded in 12-well plate and treated after 24 h with **2d** or L-**2d** in different concentrations (10, 20 or 30 nM). The day after the treatment, the plate was illuminated with visible light (light dose, 7.2 J/cm^2), and 24 h after irradiation, the cells were harvested by trypsinization and resuspended in incubation buffer containing annexin-V–fluorescein and propidium iodide. After 15 min of incubation in the dark, the cells were diluted by adding 200 μl of incubation buffer and analyzed on the BD FACSCalibur flow cytometer. A minimum of 10^4 cells for each sample were acquired in list mode and analyzed using Cell Quest software. The signal was detected by FL1 (530 nm) for annexin-V and FL2 (585 nm) for propidium iodide.

ROS were measured by cytofluorimetry. Panc-1 and BxPC-3 pancreatic cancer cells were treated with porphyrin **2b**/**2d** or L-**2b**/L-**2d** (10, 20 or 30 nM) for 24 h and then illuminated with visible light (light dose, 7.2 J/cm^2). After one day, the medium was removed, the cells were washed twice with PBS and incubated with 300 μl of 10 μM CM-H_2DCFDA (Invitrogen, USA) for 30 min in phenol red-free DMEM without serum. After two washings with PBS, the cells were trypsinized and transferred into FACS tubes containing 1 ml of PBS. The suspension was centrifuged at 1200 rpm for 3 min. The pellet was resuspended again in 300 μl of PBS, and the fluorescence was measured on the BD FACSCalibur flow cytometer.

2.5. Western Blot Assays

Protein samples were separated in 10% SDS-PAGE and blotted onto nitrocellulose membrane at 70 V for 2 h. The nitrocellulose membrane was blocked for 1 h with 5% non-fat dried milk in PBS and 0.1% Tween (Merck Life Science, MI, Italy) at room temperature. The primary antibodies used were: anti-*KRAS* (clone 3B10—2F2, mouse monoclonal, IgG mouse, Merk Life Science, Milano, Italy), anti-B-Raf (clone D9T6S, monoclonal antibody, IgG rabbit, Cell Signalling Technology, Leiden, The Netherlands), anti-pAKT (clone 193H12, monoclonal antibody, IgG rabbit, Cell Signalling Technology, Leiden, The Netherlands), anti-AKT (polyclonal antibody, IgG rabbit, Cell Signalling Technology, Leiden, The Netherlands), anti-pMEK (clone 41G9, monoclonal antibody, IgG rabbit, Cell Signalling Technology, Leiden, The Netherlands), anti-MEK (polyclonal antibody, IgG rabbit, Cell Signalling Technology, Leiden, The Netherlands), anti-pERK (polyclonal antibody, IgG rabbit, Cell Signalling Technology, Leiden, The Netherlands), anti-ERK (polyclonal antibody, IgG Rabbit, Cell Signalling Technology, Leiden, The Netherlands), anti-Nrf2 (clone D1Z9C, monoclonal antibody, IgG rabbit, Cell Signalling Technology, Leiden, The Netherlands), anti-β-actin (monoclonal antibody, IgG Mouse, Merk Life Science, Milano, Italy); anti-GAPDH (monoclonal antibody, IgG Mouse clone GAPDH-71.1, Merk Life Science, MI, Italy), anti-PARP (polyclonal antibody, IgG rabbit, Cell Signalling Technology, Leiden, The Netherlands), anti-Casp3 (polyclonal antibody, IgG rabbit, Cell Signalling Technology, Leiden, The Netherlands), anti-GPX4 (monoclonal antibody, IgG mouse, ab125066, Abcam, Cambridge, UK) . Apoptosis was triggered by using: 100 nM ADR and 1 μM AT-199 or TRAIL (2.5 ng/ml) and bortezomib (0.1 μM) (Merk Life Science, Milano, Italy) and inhibited by using Boc-D-FMK (Abcam, Cambridge, UK). The membranes were incubated overnight at 4 °C with the primary antibodies, then washed with 0.1% Tween in PBS and incubated for 1 h with the secondary antibodies conjugated to horseradish peroxidase: Anti-mouse IgG (diluted 1:5000) and anti-rabbit IgG (diluted 1:5000) (Merck Life Science, MI, Italy). The signal was developed with Super Signal® West PICO, and FEMTO (Thermo Fisher Scientific, Waltham, MA, USA) and detected with ChemiDOC XRS, Quantity One 4.6.5 software (Bio-Rad Laboratories, Segrate, MI, Italy).

2.6. Confocal Microscopy

To analyze the intracellular distribution of **2d**/L-**2d**, Panc-1 cells were seeded on 8-well polymer chambered coverslips (Ibidi GmbH, Germany, cat n° 80,826), grown for 24 h and incubated overnight with 5 μM **2d**/L-**2d** or L-Cy5 in complete DMEM in the dark. Cells were then loaded for 20 min with 2 μg/ml Hoechst and imaged in phenol red-free DMEM on a Leica TCS SP8 confocal microscope (Leica Microsystems, Germany) equipped with a stage-top environmental chamber (Okolab, Italy) and operated by Leica Application Suite X (LAS X) 3.5.5 software. Images were collected as z-stacks using a 63 x/1.4 oil immersion objective, a 405 nm diode laser (Hoechst excitation) and a tunable white-light laser (λ_{exc}: **2d**, 580 nm; Cy5, 650 nm), and are reported as maximum intensity projections.

The colocalization with organelle-specific markers was investigated on Panc-1 cells seeded on 8-well or 18-well polymer chambered coverslips (Ibidi GmbH, Germany, cat. n° 80,826 and 81,816) and incubated for 24 h with 3 μM **2d**/L-**2d** in the dark. Cells were then labeled for 30 min with 100 nM MitoTracker Green or 75 nM LysoTracker Green DND-26 (Invitrogen, Walthman, MA, USA) in the presence of 2 μg/ml Hoechst prior to in vivo confocal analysis on a Leica TCS SP8 microscope with environmental control. Alternatively, **2d**/L-**2d**-treated cells were fixed with 3% PFA and immunolabeled with anti-LAMP1 (clone D2D11, monoclonal antibody, IgG rabbit, monoclonal antibody, IgG Mouse, Merk Life Science, MI, Italy) or anti-KDEL (rabbit monoclonal, IgG rabbit, abcam, Cambridge, UK) primary antibodies followed by Goat Anti-Rabbit IgG AlexaFluor 488-conjugated secondary antibody (abcam, Cambridge, UK). Nuclei were counterstained with Hoechst. Single optical sections were acquired using 63×/1.4 (MitoTracker, LysoTracker) or 100×/1.4 (LAMP1, KDEL) oil objectives with excitation at 405 nm for Hoechst, 490 nm for MitroTracker and LysoTracker, 495 nm for AlexaFluor 488, and 580 nm for **2d**.

For in vivo lipid peroxidation assay, Panc-1 cells were seeded on glass dishes (WillCo Dishes 5040, WillCo Wells, Amsterdam, The Netherlands) and treated after 12 h with **2d**/L-**2d** (40 nM) in the dark. After 24 h, cells were irradiated or treated with Erastin (Sigma-Aldrich, MO USA) and loaded with 2 μM c-11 bodipy $^{581/591}$ (LifeTechnologies, CA, USA) and 10 μg Hoechst (Sigma-Aldrich, MO USA). The 591/510 emission shift was observed for 15 h by acquiring images every 10 min. Images were collected as z-stacks using a 63 x/1.4 oil immersion objective and a costant laser power was used for the four experimental conditions compared. ROI quantification tool (LASX) was used for the quantification, GraphPad prism for the analysis.

Images were deconvolved using Huygens Essential version 18.10 software (Scientific Volume Imaging, the Netherlands). Fluorescence intensity profiles were measured along a 25 μm-line using Leica Application Suite X (LAS X) 3.5.5. Each profile was normalized to its maximum peak intensity.

2.7. Statistics

Data are reported as mean values ± standard error (SE). Statistical analyses were carried out by using Sigma Plot software. Group differences were analyzed by Student's *t*-test. Groups are considered different when $P < 0.05$.

3. Results and Discussion

3.1. Preparation and Characterization of Porphyrin-Engrafted Liposomes

Palmitoyl-2-oleoyl-sn-glycero-3-phosphocholine (POPC) liposomes were obtained by extruding 10 times a 10 mM POPC solution in PBS through a 50 nm diameter polycarbonate membrane using N_2 at 35–40

bar [23]. The liposomes analyzed by Nanoparticle Tracking Analysis (NTA) gave an average diameter of 85 ± 1 nm (Fig. 1A-C), which did not practically change upon functionalization with the alkyl porphyrins (not shown). Porphyrins **2b** and **2d** have been synthesized as previously described [13] (Fig. 1D). Both have similar excitation/emission spectra in PBS. Typical excitation/emission spectra of porphyrin **2d** are shown in Fig. 1E. The emission spectra show that the fluorescence of 1.25 μM free **2d** is strongly quenched due to π-stacking interactions between the porphyrin planar macrocycles. The addition of POPC liposomes strongly increases the fluorescence intensity (spectrum after 10 min), which levels off with time (spectrum after 50 min). This is due to the fact that upon binding to the liposome, the porphyrins dissagregate and their quantum yield for fluorescence increases. The alkylated porphyrins efficiently bind to POPC liposomes (Fig. 1F), as determined independently by size-exclusion HPLC and Surface Plasmon Resonance (SPR) assays. The HPLC chromatograms in Fig. 1G showed that when 0.1 mM **2d** were injected alone on the size-exclusion column, the porphyrin fluorescence was not visible, as observed with **2b**, as a result of aggregation-related quenching. At a concentration of 10 μM a faint signal appeared. But when **2d** was mixed with POPC liposomes at 0.1 mol% (10 μM **2d**, 10 mM POPC), fluorescent liposomes were observed, eluting at the same time as the control empty liposomes, in nice agreement with fluorescence spectra. A similar behavior was obseserved with porphyrin **2b** at 1 mol% (100 μM **2b**, 10 mM POPC) (Fig. S2). These results are corroborated by the SPR data obtained with **2b** and **2d**, where an increase in detector response proportional to the concentration of the alkylated porphyrin was observed. Fig. 1H shows typical SPR curves obtained with **2d**. Upon binding, in the SPR flow-cell the liposome bilayers are expected to saturate in guest molecules (**2d**) to a steady state level, according to their concentration in the flow. At concentrations >5 μM, the response increased non-linearly for the data points at 10 and 20 μM, which again indicates the presence of aggregates. In fact, if **2d** forms aggregates, its interaction with POPC liposomes would fix on the liposome surface a higher amount of porphyrin so that the SPR response is expected to be higher. The binding was proportional to **2d** concentration but did not approach saturation, indicating that the liposomes have a very high loading capacity. The stability of **2d** engraftment during the dissociation phase on SPR was very high (approximately 80% of the maximal binding level after 550 s). We also performed experiments with **2b** and found that even higher amounts of porphyrin (50 μM) can efficiently bound to the liposomes without reaching saturation (Fig. S3).

Next, we measured the production of ROS by **2b**/L-**2b** and **2d**/L-**2d** in pancreatic Panc-1 and BxPC3 cancer cells, using CM-H_2DCFDA, which is non-fluorescent in the reduced state. When the probe is oxidized by cellular ROS and its acetate group removed by esterases, it becomes fluorescent. Fig. 1I shows that the fluorescence, measured by FACS, of Panc-1 and BxPC3 cells treated with **2d**, either in free form or engrafted into POPC liposomes (L-**2d**) increases in a dose-response manner. The experiment was performed also with **2b** and L-**2b**, which showed a lower ROS-generating capacity, probably because they enter into the cells less efficiently than **2d** and L-**2d**.

3.2. Uptake and Intracellular Distribution of Free and Liposome-Bound Alkyl Porphyrins

As the tetrapyrrole macrocycle of the porphyrins emits red fluorescence when excited at 488 nm, the uptake of porphyrins **2b** and **2d** was investigated by FACS (Fig. 2A). Both porphyrins, **2b**/**2d** and L-**2b**/L-**2d**, enter efficiently in pancreatic cancer cells. According to the fluorescence emitted by the porphyrins (Ex 488 nm, Em 660 nm), **2d**/L-**2d** with a C18 chain is taken up ~5-times more than **2b**/L-**2b** with a C14 chain. Due to its higher uptake, in this study we focused mostly on **2d**/L-**2d**. We found that **2d** and L-**2d** are taken up almost with the same efficiency by Panc-1 and MiaPaCa-2 cells, while in BxPC3 cells the uptake of L-**2d** is ~20% higher than that of free **2d** (Fig. S4). An insight into the mechanism by which **2d** and L-**2d** penetrate the cell membrane was obtained by treating the cells with dynasore, a noncompetitive inhibitor of dynamin GTPase activity, which blocks clathrin-mediated endocytosis [24]. Fig. 2B-F shows that dynasore reduces the uptake of L-**2d** in Panc-1, BxPC3 and MIA-PaCa pancreatic cancer cells by ~45%, 20%, 50%, respectively, while free **2d** by ~55%, 30%, 70% (Fig. S4). We also tested cytochalasin, an inhibitor of micropinocytosis [25], finding that it did not have any impact on the uptake. Together, these experiments suggest that endocytosis is a mechanism through which **2d** and L-**2d** are internalized in Panc-1 cells.

We also performed confocal microscopy experiments to investigate how **2d** and L-**2d** distribute within the cell. Fig. 2G shows maximum intensity projections of living Panc-1 cells treated with free **2d** and L-**2d**. The nucleus of the cells was stained with Hoechst, while the porphyrin was visualized through its red fluorescence emitted upon excitation at 580 nm. The merge panel shows that free **2d** locates in the membrane lipid bilayer, owing to its lipophilic chain, and also in the cytoplasm, with a punctuated distribution. This suggests that **2d** is internalized by an active (endocytosis) and, to a lesser extent, also by passive a (membrane fusion) mechanism of transport. The fraction of **2d** following the endocytic pathway is trapped into endosomes, which account for the observed punctuated pattern. Most endosomes lay in the cytoplasm, but some seem to co-localize with the nucleus (pink dots). By contrast, L-**2d** seems to be taken up only by endocytosis, showing a robust punctuated cytoplasm distribution. The images did not show any location of L-**2d** in the membrane. Fig. 2H shows Panc-1 cells treated with POPC liposomes marked with Cy5.5, encapsulated in the central core of the nanoparticle. The merge image shows a punctuated distribution similar to that shown in Fig. 2G, where the liposomes where stained by the porphyrin**.** The two different staining methods gave the same distribution pattern according to which the liposomes are predominantely localized in the cytoplasm and slightly in the nucleus. The punctuated distribution of **2d** and L-**2d** suggested us to investigate if they target specific organelles (Fig. 3A-F). Micrographs of living Panc-1 cells treated with free **2d** or L-**2d** and stained with MitoTracker Green are presented in Fig. 3A, B. Individual channel images of porphyrin **2d** or L-**2d** and MitoTracker green are shown in grey scale, while the merge panel is reported in colour. The images show that the porphyrin, either free or engrafted into the liposomes, does not co-localize with the mitochondria, as demonstrated by the fact that the fluorescence intensity profiles of **2d**/L-**2d** and Mito Tracker green, along a fixed straight line, do not overlap. We then asked if there is co-localization between the porphyrins and lysosomes by using LysoTracker green. When we carried out the experiment with living cells, the LysoTracker green fluorescence was strongly quenched by **2d**/L-**2d**, suggesting that LisoTracker and the porphyrin co-localize and interact with each other (not shown). However, to directly demonstrate that **2d** and L-**2d** target the lysosomes, we treated living Panc-1 cells with the porphyrin, we then fixed the cells and immunolabeled them with LAMP-1 antibody, specific for the lysosomal-associated membrane protein 1 residing across the lysosomal membranes [26]. The merge panel and the fluorescence intensity plots of Fig. 3C show that free **2d** strongly co-localizes with the lysosomes: the yellow foci indicate co-localization between **2d** and lysosomes (Fig. S5 shows a magnified image). The fluorescence intensity plots show that L-**2d** co-localizes with lysosomes only partially, as most L-**2d** remains trapped into endosomes. Finally, we tested if **2d** and L-**2d** co-localize with the endoplasmic reticulum (ER) (Fig. 3E, F). We stained ER with KDEL antibody recognizing Lys-Asp-Glu-Leu (KDEL) at the carboxy-terminus of soluble endoplasmic reticulum (ER) resident proteins [27]. ER shows an intense staining spreading over the whole cytoplasm. The fluorescence intensity plots show that there is no overlapping between KDEL and **2d**. Indeed, free **2d** is accumulated in an area where the ER signal is more rarefied (most probably occupied by the lysosomes). Instead, L-**2d** shows a slight co-localization with ER. To sum up, we can state that: (i) free **2d** is transported into Panc-1 cells via endocytosis and passive diffusion; it localizes in the membrane as well as in the cytoplasm; in this latter case, it co-localizes with lysosomes but not with

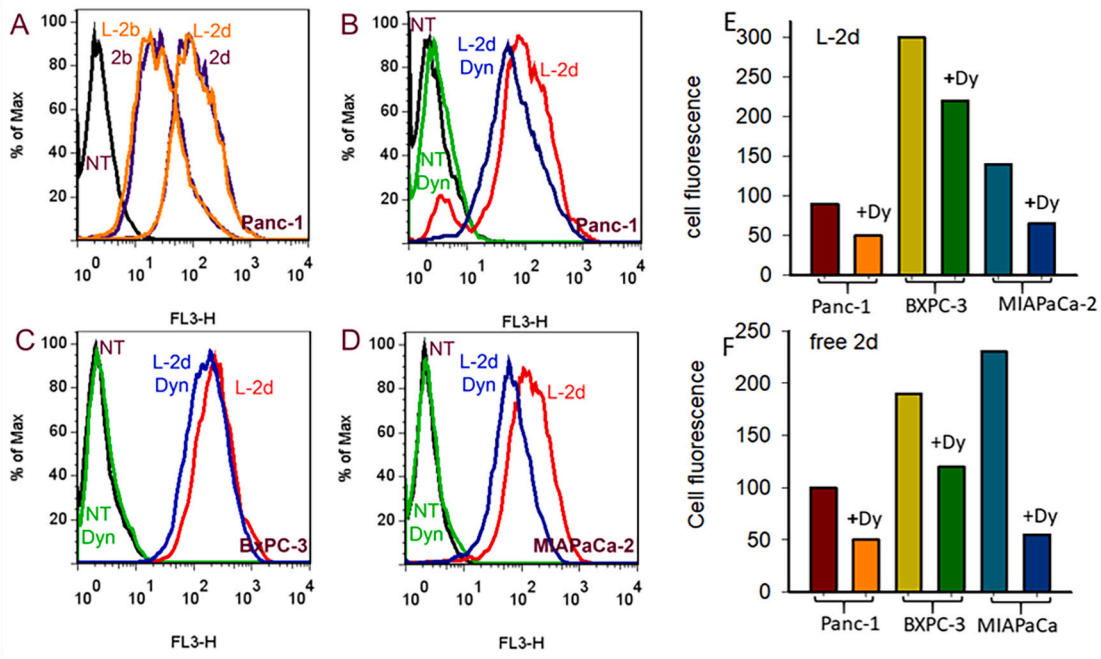

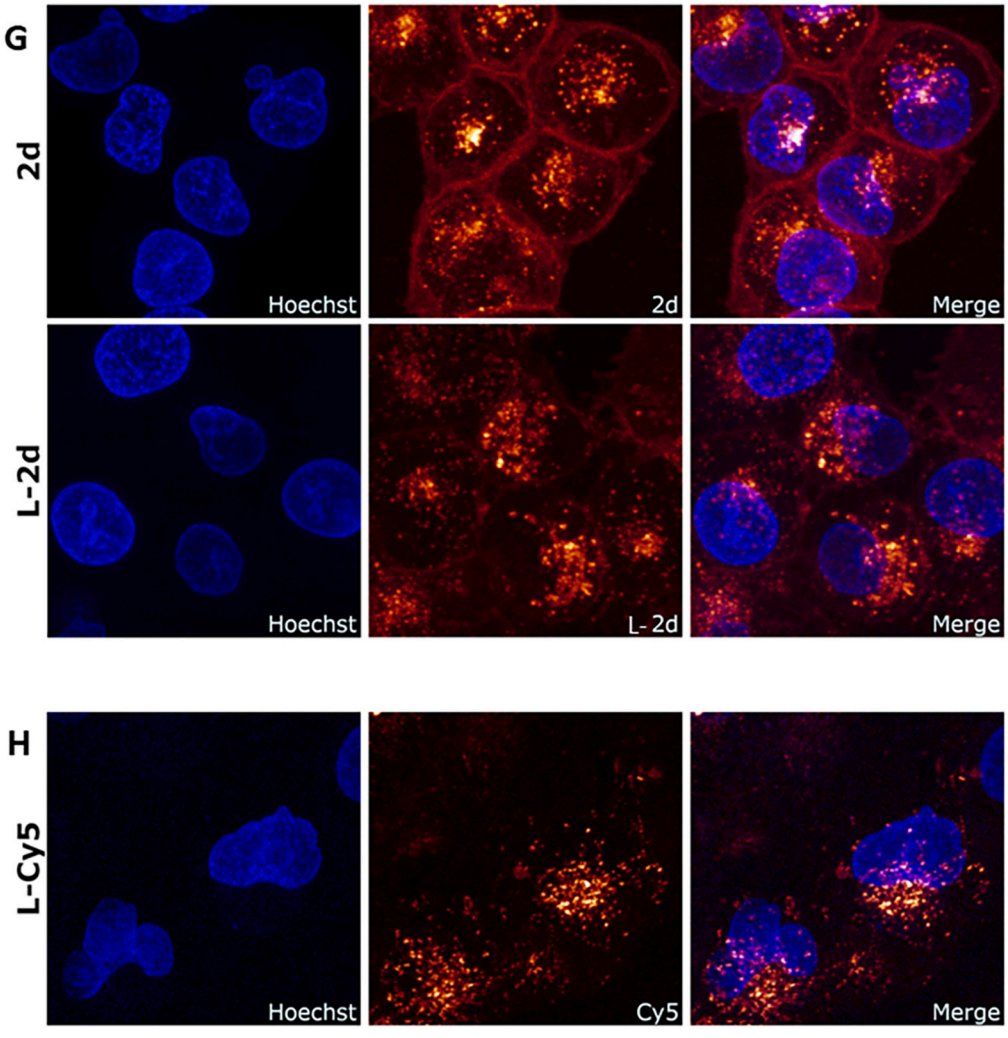

(caption on next page)

Fig. 2. (A) FACS analyses of Panc-1 cells treated with 1 μM free **2d**/**2b** or L-**2d**/L-**2b** for 6 h; (B–D) FACS of Panc-1, BxPC3 and MIA PaCa cancer cells treated with free **2d** or L-**2d** for 6 h in the presence and absence of dynasore; (E, F) Bar plots reporting the fluorescence of the cells terted with the L-**2d** in the absence and presence of dynasore; (G) Confocal microscopy images of living Panc-1 cells treated overnight with 5 μM **2d** and L-**2d**. The nuclei of the cells have been stained with Hoechst (blue), while porphyrins **2d** is visualized through its red emission. The merge images are also shown; (H) Living Panc-1 cells have been treated with POPC liposomes marked with Cy5 encapsulated in the central core of the liposomes (Hoechst, blue; Cy5, glow). The images show the distribution of Cy5-labeled liposomes in Panc1-cells. All the images are maximum intensity projections of confocal z-stacks spanning the entire cell. (For interpretation of the references to colour in this figure legend, the reader is referred to the web version of this article.)

mitochondria and ER; (ii) L-**2d** is instead taken up by endocytosis only, showing endosome particles in the cytoplasm, partly colocalizing with lysosomes and ER.

3.3. Free Porphyrin 2d Downregulates the KRAS-Nrf2 axis while Liposome-Bound Porphyrin L-2d Does Not

In general, cancer cells produce more ROS than normal cells, due to a higher metabolic rate and hypoxia conditions [28]. As high levels of ROS can cause oxidative damage to DNA, RNA and phospholipids, they are controlled through a sophisticated detoxifying system involving Nrf2 and enzymatic antioxidants [29–31]. As illustrated in Fig. 4A, the redox homeostasis in PDAC cells is controlled by the *KRAS*-Nrf2 axis. ROS stimulate *KRAS*, which in turn upregulates Nrf2: a ROS sensor gene that activates the cellular antioxidant response [29,30,32]. The *KRAS*-Nrf2 axis prevents the accumulation of ROS that could otherwise inhibit proliferation. When the cells are treated with porphyrin **2d** and light, intracellular ROS increase dramatically, via a type II photodynamic mechanism [33] (Fig. 4B). Although ROS stimulate the *KRAS*-Nrf2 axis, we observed a downregulation of *KRAS* and Nrf2 because free **2d** located in the cytopasm binds to *KRAS* mRNA, at G4 structures located in the 5′-untraslated region [13]. Upon irradiation, the porphyrin produces ROS and $^1O_2$ that degrade mRNA and thus suppress *KRAS* translation. The effect of **2d** in free form on *KRAS* is clearly seen in Fig. 4D–I, which shows that 48 h after irradiation, *KRAS* is reduced in a dose-response manner in Panc-1 and BxPC3 cells to ~30% of the control (non-treated cells). The suppression of *KRAS* results in the downregulation of Nrf2 (Fig. 4J, left), and thus in the loss of the control mediated by Nrf2 of the ROS homeostasis. Under these conditions, ROS increase dramatically and induce cell death. Interestingly, a different picture was observed when the cells were treated with L-**2d** and light. In this case, *KRAS* was upregulated in BxPC3 cells at both 24 and 48 h, while in Panc-1 cells only at 24 h. This suggests that the porphyrin engrafted into the liposomes is unable to bind to *KRAS* mRNA and suppress the gene. This correlates with the finding that L-**2d** only partly follows the endosome-lysosome pathway, differently from free **2d**. Most of L-**2d** is likely to remain engrafted into the liposomes, from where the porphyrin does not easily spread into the cytoplasm as molecule in free form capable to interact with G4 structures in *KRAS* mRNA. Upon illumination with visible light, L-**2d** generates ROS and $^1O_2$ that stimulate the *KRAS*-Nrf2 pathway (Fig. 4H–J), as occurs when the cells are treated with H_2O_2 [19,34]. As ROS generated by L-2d overcome the detoxification capacity of the cells, their accumulation induces apoptosis.

Next, it is known that in *KRAS*-driven pancreatic cancers, the signalling passes through the Mek/Erk and PI3K/Akt pathways [35]. Recent studies have demonstrated that the initiation, maintenance and progression of PDAC depend more on the PI3K/Akt pathway [36,37]. Given that cancer cells produce relatively high levels of oxidative stress, ROS play a critical role in cell growth and survival [38,39]. ROS affect *KRAS* signalling in a rather complex way. First, ROS act directly on Akt by promoting a conformational change through the formation of an intramolecular disulphide bond that causes dephosphorylation and inactivation of Akt [40,41]. This means that the large amount of ROS produced by the photoactivated porphyrin induces the dephosphorylation of Akt, the blockage of downstream pathway and inhibition of cell proliferation. By contrast, enhanced ROS generally leads to activation of the Mek/Erk pathway by a mechanism which is still unclear but probably going through the inactivation of MKPs and/or ROS-mediated modifications of Merk/Erk signalling proteins [42]. We examined by Western blots the status of the two signalling pathways in Panc-1 cells treated with the porphyrins (Fig. 4L). We found, indeed, that the ROS-generated by **2d** and L-**2d** have an opposing effect on the two pathways: the porphyrin strongly reduces P-Akt, and increases P-Mek and P-Erk in a dose-response manner. This behavior fits with the observation that the Raf/Mek/Erk pathway is activated by ROS, in a *KRAS*-independent manner [37,38]. A similar result was obtained with porphyrin **2b** (Fig. S6). As PI3K/Pdk1/Akt is the main proliferation pathway in PDAC, its inhibition by photoactivated **2d** and L-**2d** should result in a significant drop of cell proliferation.

3.4. Effect of Free and Liposome-Bound Alkyl Porphyrins on Cell Viability and Colony Formation

To evaluate the photosensitization of free or liposome-bound porphyrins **2d** and **2b**, we measured their potency to kill pancreatic cancer cells by performing cell viability assays with resazurin, a non-fluorescent phenoxazine that is reduced in fluorescent resofurin, in living and metabolically active cells.

The porphyrins were tested in Panc-1 and MIA PaCa cells, which are *KRAS* and *TP53* mutated, and in BxPC-3 cells which are only TP53 mutated. When the cells were treated in the dark with increasing amounts of L-**2d** (10, 20 and 30 nM) or free **2d**, no effect on viability was observed (typical behavior obtained with L-**2d** is shown in Fig. 5A). By contrast, upon treatment with visible light (7.2 J/cm^2) a dose-response decrease in viability was observed (Fig. 5B). By plotting the % viability at 48 h after illumination, as a function of porphyrin concentration, we found that the IC_{50} for **2d** and L-**2d** are 20.8 ± 0.6 and 19.1 ± 0.8 nM for Panc-1 cells; 25.8 ± 1.0 and 29.1 ± 1.4 nM for BxPC3 cells; 21.9 ± 1.1 and 23.5 ± 1.2 nM for MIA PaCa cells. The data show that there is little difference in phototoxicity between **2d** and L-**2d.** A similar behavior was detected with **2b** (Fig. S7).

To assess the effect of **2d** and L-**2d** on cell proliferation, we carried out a clonogenic assay with Panc-1 and BxPC3 cells (Fig. 5C, D). The cells were seeded at a dilution that a single colony could be formed by each cell. After 15 days of growth, the colonies of at least 50 cells were counted and the results reported in a bar plot. The number of colonies in the untreated and porphyrin-treated plates in the dark was the same, confirming that without photoactivation the porphyrins are not toxic. In contrast, after light treatment (7.2 J/cm^2), **2d** and L-**2d** strongly reduced the number of colonies in both types of cells. The bar plots show that 20 nM **2d**, reduced Panc-1 and BxPC3 colonies by ~50% and 70%, respectively, while L-**2d** by 70% in both types of cells. A similar result was obtained with Panc-1 cells treated with **2b** and L-**2b** (Fig. S8).

We then carried out annexin V–propidium iodide assays. In the early stage of apoptosis, the cell membrane loses its phospholipid asymmetry. Phosphatidylserine (PS) jumps into the outer leaflet of the membrane. Annexin V-FITC binding to PS can mark the cells in early apoptosis. In late apoptosis (LA), the plasma membrane is ruptured and PI can bind to intracellular DNA. The cells are stained by both PI and Annexin V. Fig. 6A, B shows a cell cytometry analysis performed on Panc-1 and BxPC3 cells treated with **2d**/L-**2d** and light. The results are reported in **Supplementary S9**. The percentage of apoptotic cells in the control (cells untreated with the porphyrin and illuminated with visible light) varies from 10 to 15%. The cells treated with empty liposome (L) and light did not induce apoptosis compared to control (nontreated cells). Instead, L-**2d** induced a strong apoptotic response, in a dose-response

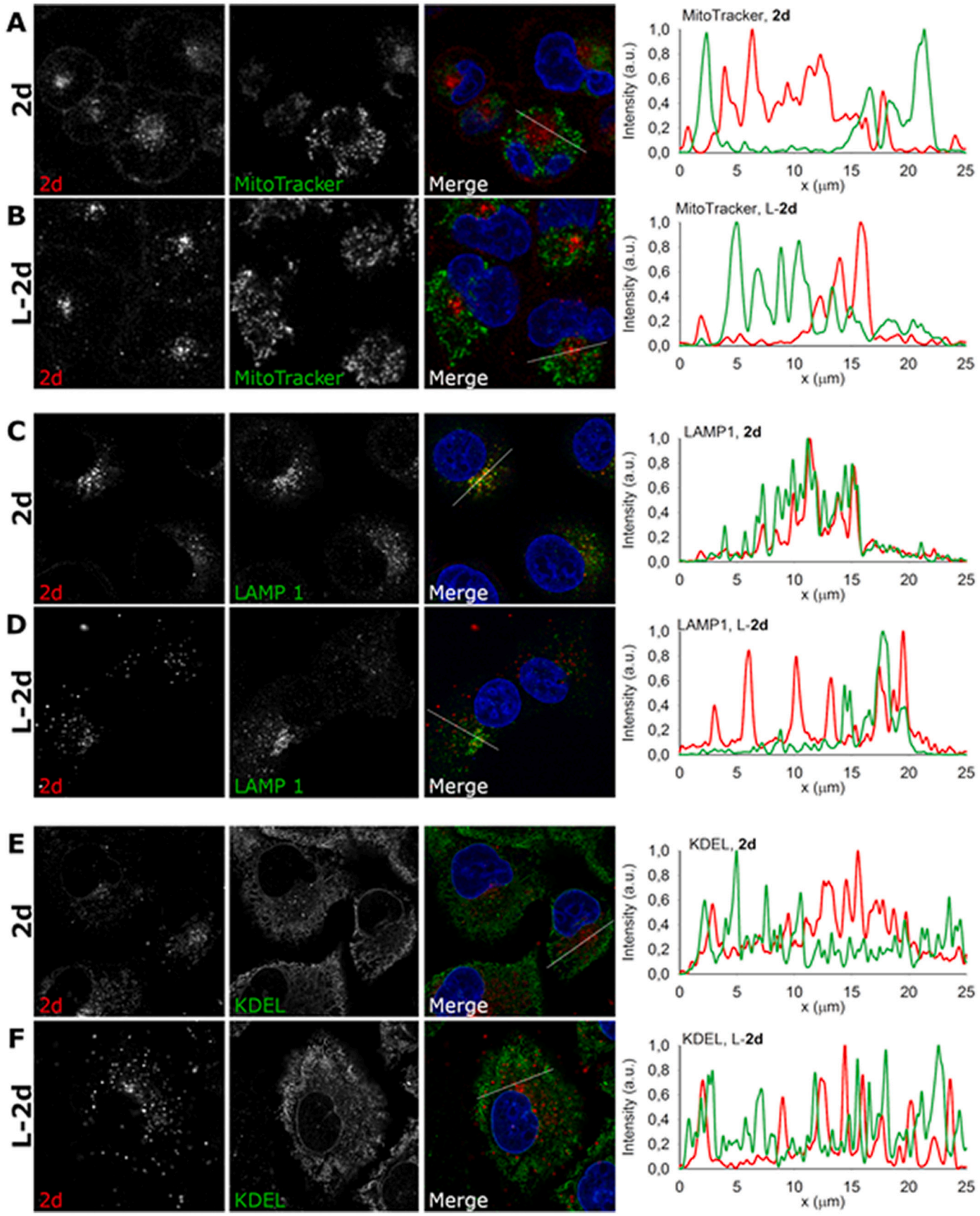

Fig. 3. (A) Confocal microscopy Fluorescence microscopic images of Panc-1 pancreatic cancer cells, co-treated with Hoechst, **2d**/L-**2d**, MitoTracker, LAMP 1, KDEL. The fluorescence intensity plots show **2d** or L-**2d** co-localization with the organelles.

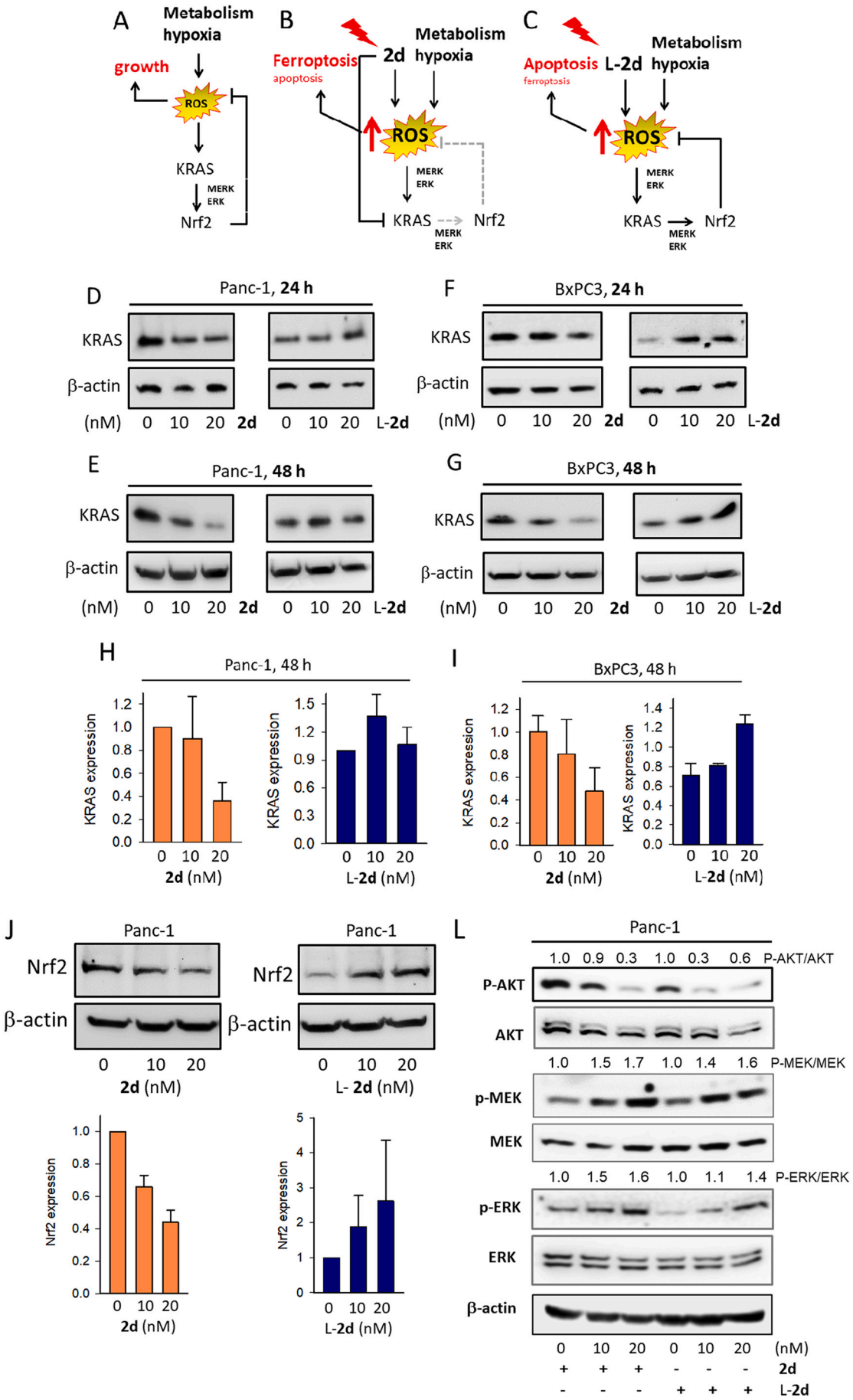

(caption on next page)

Fig. 4. (A-C) Schemes showing the *KRAS*-Nrf2 axis and the effect of porphyrin **2d** and L-**2d** on pancreatic cancer cells; (D—I) Western blots showing the expression of *KRAS* and β-actin in Panc-1 and BxPC3 cells 24 and 48 h after photo-treatment with porphyrin **2d** and L-**2d.** Panc-1 data are the average of two independent experiments. The data are the average of 2 independent experiments; (J) Expression of Nrf2 in Panc-1 cells treated with **2d**/L-**2d** and light. The data are the average of 2 independent experiments; (L) Activation of the Mek-Erk and PI3P-Akt pathways in Panc-1 cells treated with **2d** and L-**2d**.

manner, in both cell lines. The percentage of early and late apoptotic cells is 87% in Panc-1 and 75% (±10%) in BxPC3 cells, after treatment with 30 nM L-**2d**. By contrast, **2d** is less effective in promoting apoptosis: 30 nM **2d** induced apoptosis in 42% Panc-1 and 56% Bx PC3 cells (±10%). Collectively, the data show that L-**2d** is 2-fold stronger in inducing apoptosis than free **2d**.

3.5. The Alkyl-Porphyrins Activate a Complex Cell Death Involving Ferroptosis and Apoptosis

Recent studies have demonstrated that lipid peroxidation can trigger a new type of programmed cell death named ferroptosis. It was first proposed by Dixon [43] in 2012 as a new cell death caused by an iron-dependent accumulation of lethal lipid ROS. Morphologically, ferroptotic cells show a normal size nucleus in which DNA is not fragmented, a reduced mitochondrial volume and no rupture of the cell membrane. The process is inhibited by iron chelators but not by caspase inhibitors [44]. Confocal microscopy showed that only a fraction of porphyrin-treated cells exhibited the typical features of apoptosis: i.e. a rounding morphology and blebbing of the plasma membrane. Therefore we asked if our alkyl-porphyrins induce a mixed type of cell death, as observed with lung cancer cells treated with PdPT [45]. To provide evidence that the alkyl-porphyrins promote ferroptosis, we compared the behavior of **2d** and L-**2d** with erastin, a strong ferroptotic agent [46], in the presence and absence of ferrostatin 1 (Fer-1), an inhibitor of ferroptosis [47], or BocD-fmk, a broad range caspase inhibitor [48]. Fig. 7A, B shows that **2d** up to 40 nM strongly reduced the viability of Panc-1 cell in a dose response manner, after light treatment (7.2 J/cm^2). As expected, the treatment with erastin (15 μM) showed a dramatic drop in cell viability, attributed by us to ferroptosis. The cell viability was completely restored when the cells were co-treated with erastin (15 μM) and Fer-1 (15 μM). Analogously, Fer-1 strongly

rescue the viability also in Panc-1 cells treated with 20 or 40 nM **2d**, suggesting that the porphyrin too induced cell death by ferroptosis, as observed with porphyrin TPP loaded nanoparticles in B16 melanoma cells.[49] However, as Fer-1 did not fully recover the viability in the cells treated with 40 nM **2d**, in addition to ferroptosis the porphyrin activates apoptosis, in keeping with the FACS data. We then inhibited apopotosis with Bocd-fmk and found that the percentage of viable cells following a treatment with 20 and 40 nM **2d** was ~80% and ~ 50%, respectively, compared to control (untreated cells). This reduction in viability is due to ferroptosis. Together, the data indicate that free **2d** triggers a mixed mechanism of death: apoptosis and ferroptosis. We roughly estimated that 40 nM **2d** promotes ~50% ferroptosis and ~ 40% apoptosis. In Fig. 7B we report the results obtained with the liposome-bound porphyrin L-**2d**. The rescue in viability promoted by Fer-1 in Panc-1 cells treated with 40 nM L-**2d** was ~20%, suggesting that L-**2d** is a weaker ferroptotic activator than free **2d**. In this case we estimated that 40 nM L-**2d** promoted cell death by ferroptosis in 20% of the cells and apoptosis in 70% of the cells. A qualitatively similar result was observed with BxPC-3 cells (Fig. S10) and with **2b** (Fig. S11). Consistent with these data is the finding that **2d,** binding to the membranes, oxidizes the phospholipids, generating lipid ROS that trigger ferroptosis. To support this, we used C11-bodipy $^{581/591}$: a fluorescent ratio probe that allows to measure and visualize lipid peroxidation in living cells [50]. Its fluorescence shifts from red (maximum at 595 nm) to green (maximum at 520 nm) when the probe is challenged with oxidizing species [51]. Fig. 7C shows the fluorescence ratio as a function of time for a single cell loaded with C11-bodipy $^{581/591}$ and **2d** or L-**2d**. The analysis was extended to a number of cells varying from 11 to 27. It can be seen that **2d** (40 nM) increases the oxidized/reduced (510/591 nm) ratio of C11-bodipy $^{581/591}$ 2-fold more than L-**2d**, over a period of 15 h since light treatment, consistently with the finding that free **2d** binds to the membrane, while L-**2d** does not or does it in little amount. Note that erastin showed an oxidizing capacity similar to that of L-**2d** and about half of that induced by **2d.** In Fig. S12 we report Panc-1 cells treated for 15 min, 6 and 12 h with C11-bodipy $^{581/591}$ and porphyrins **2d** or L-**2d**. It can be seen that in the absence of porphyrin, the fluorescence of C11-bodipy $^{581/591}$ does not shift from red to green. In contrast, a fluorescence shift occurs in 6 h with **2d**, 12 h with L-**2d** or erastin.

Next, we investigated the extent of apoptosis triggered by the porphyrins. Fig. 7D, E shows that, compared to untreated cells, 40 nM **2d** and L-**2d** increase the fluorescence of *Z*-DEVD R110 by ~1.5- and 3-fold, respectively, suggesting that the porphyrin induces some caspase 3/7 activity. We then co-treated Panc-1 cells with **2d**/L-**2d** and Fer-1: under these conditions ferroptosis is inhibited and the cells die by apoptosis only. It can be observed that 40 nM **2d** + Fer-1 increase the Z-DEVD R110 fluorescence by 2.9-fold, while 40 nM L-**2d** + Fer-1 increase the fluorescence by 6-fold, suggesting that the inhibition of ferroptosis is compensated by an increase of apoptosis. Collectively, the data show that caspase 3/7 is more active in Panc-1 cells treated with L-**2d** than with **2d**, in agreement with FACS and cell viability assays. To confirm this behavior, we carried out Western blot experiments (Fig. 7F, G). It can be seen that L-**2d** induced more cleavage of PARP-1 and procaspase 3 than **2d** does, attesting that the porphyrin delivered with liposomes behaves more as a pro-apoptotic than ferroptotic compound.

Given the evidence that **2d** stimulates ferroptosis, we focused on GPX4, as previous studies have demonstrated that its depletion results in excessive lipid peroxidation and ferroptotic cell death [52,53]. Indeed, GPX4 is a phospholipid hydrogenperoxide glutathione peroxidase that catalyzes the reduction of lipid hydrogenperoxides in order to protect the cells against oxidative damage. Fig. 7H shows that photoactivated **2d** strongly suppresses GPX4 while L-**2d** does not. This is in keeping with the finding that **2d** induces mainly ferroptosis while L-**2d** induces mainly apoptosis. A similar behavior was observed with **2b** and L-**2b** (Fig. S13).

Finally, further support that free **2d** induces ferroptosis was obtained by a clonogenic assay (Fig. 7I, J). It can be seen that a 20 nM **2d** reduces the number of colonies to 25% of control (untreated cells). This strong inhibitory effect is nearly suppressed by Fer-1, consistently with the fact that **2d** significantly inhibits cell growth by ferroptosis.

4. Conclusion

The cationic alkyl-porphyrins **2b** and **2d** show an excellent photodynamic effect in PDAC cells, either as molecules in free form or engrafted into POPC liposomes. While the free alkyl- porphyrins penetrate the cell membrane by an active (endocytosis) and to a lesser extent by a passive (membrane fusion) transport, liposome-engrafted porphyrins are taken up by endocytosis only.

Confocal microscopy experiments showed that **2d** co-localizes with the lysosomes, from which it is released into the cytoplasm where it binds to and degrades upon illumination *KRAS* mRNA [13]. In contrast, when the porphyrin is delivered engrafted into liposomes (L-**2d**), it co-localizes only partially with the lysosomes, which presumably release into the cytoplasm a limited amount of porphyrin insufficient to suppress *KRAS*. Interestingly, this unexpected behavior affects the type of cell death mediated by the porphyrins. Indeed, the suppression of *KRAS* in Panc-1 cells results in the downregulation of Nrf2 and GPX4, which protects membrane lipids from peroxidation (GPX4 is among the targets

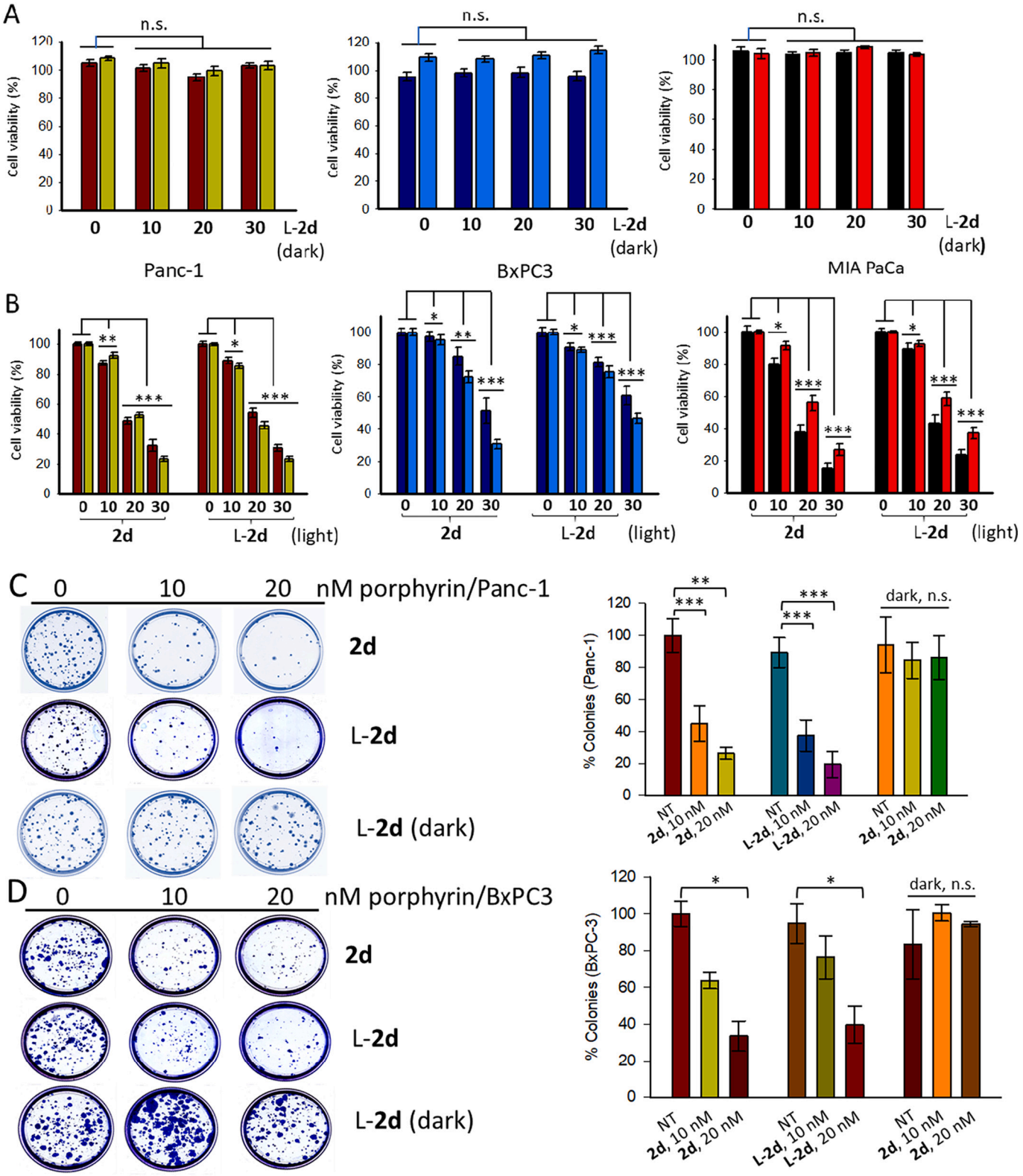

Fig. 5. (A, B) Cell viability (% values compared to cells treated only with light) of PDAC cells treated with 0, 10, 20, 30 nM L-**2d** in the dark or 0, 10, 20, 30 nM **2d** and L-**2d** after illumination with visible light (light dose, 7.2 J/cm^2). The assays were performed 24 (brown, blue and black bars) and 48 h (green, sky blue and red bars) after illumination. The data are the average of: 3 independent experiments, 7 replicates each with Panc-1; 2 experiments, 7 replicates with BxPC3; 1 experiments, 7 replicates with MIA PaCa-3. Statistical significance respect to untreated cells: $P \leq 0.05$ (*), 0.01 (**), 0.001 (***); (C, D) Clonogenic assays with Panc-1 and BxPC3 cells treated with **2d** or L-**2d** and visible light (light dose, 7.2 J/cm^2). Number of colonies was determined 15 days after illumination. Data are the average of one experiment in triplicate. Statistical significance respect to untreated cells: P $\leq$ 0.05 (*), 0.01 (**), 0.001 (***).

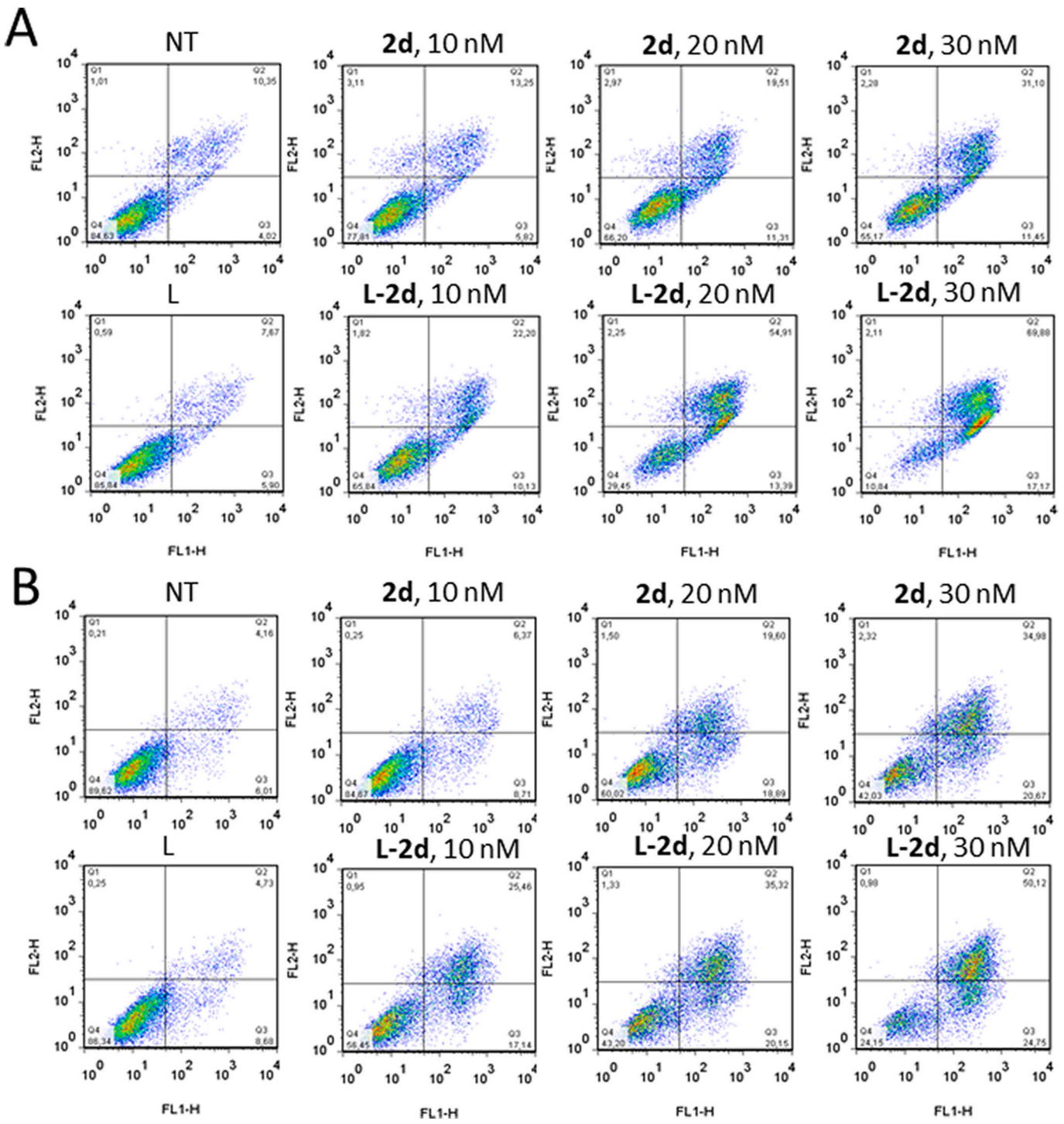

Fig. 6. Annexin-propidium iodide assay with Panc-1(top) and BxPC3 (bottom) cells treated with 0, 10, 20 and 30 nM **2d**/L-**2d** and light. Percentage of early and late apoptotic cells (Q2 + Q3) is reported in **Supplementary S9** (Table). FL1-H = annexin V, FL2-H = propidium iodide.

of Nrf2 [54]). Therefore, we think that the inhibition of the *KRAS*-Nrf2-GPX4 axis should dramatically lower the capacity of the cell to reduce lipid peroxidation and protect the membranes. Under these stress conditions, the oxidized membrane liberates lipid ROS that activate cell death by ferroptosis (Fig. 8A, B). By contrast, the porphyrin bound to the liposomes (L-**2d)** internalizes into cancer cells by endocytosis, without leaving enough porphyrin molecules in the lipid bilayer to generate lipid ROS. In the cytoplasm L-**2d** does not release sufficient porphyrin molecules to suppress *KRAS* [13] and its axis with Nrf2 and GPX4. L-**2d** is therefore a weak activator of ferroptosis. However, L-**2d** is found to efficiently generate ROS upon illumination, which strongly induce cell death by apoptosis.

To sum up, our results show that the mechanism of cell death induced by the cationic alkyl-modified porphyrins is complex, as it is based on ferroptosis and apoptosis. The two types of cell death co-exist in porphyrin treated cells and the prevalence of one over the other is in relationship with the delivery mode: liposome-engrafted alkyl-porphyrin promotes mainly apoptosis while free alkyl-porphyrin promotes mainly ferroptosis. Our study provides new insights into the type of cell death induced by alkyl porphyrins, which are useful for a rational

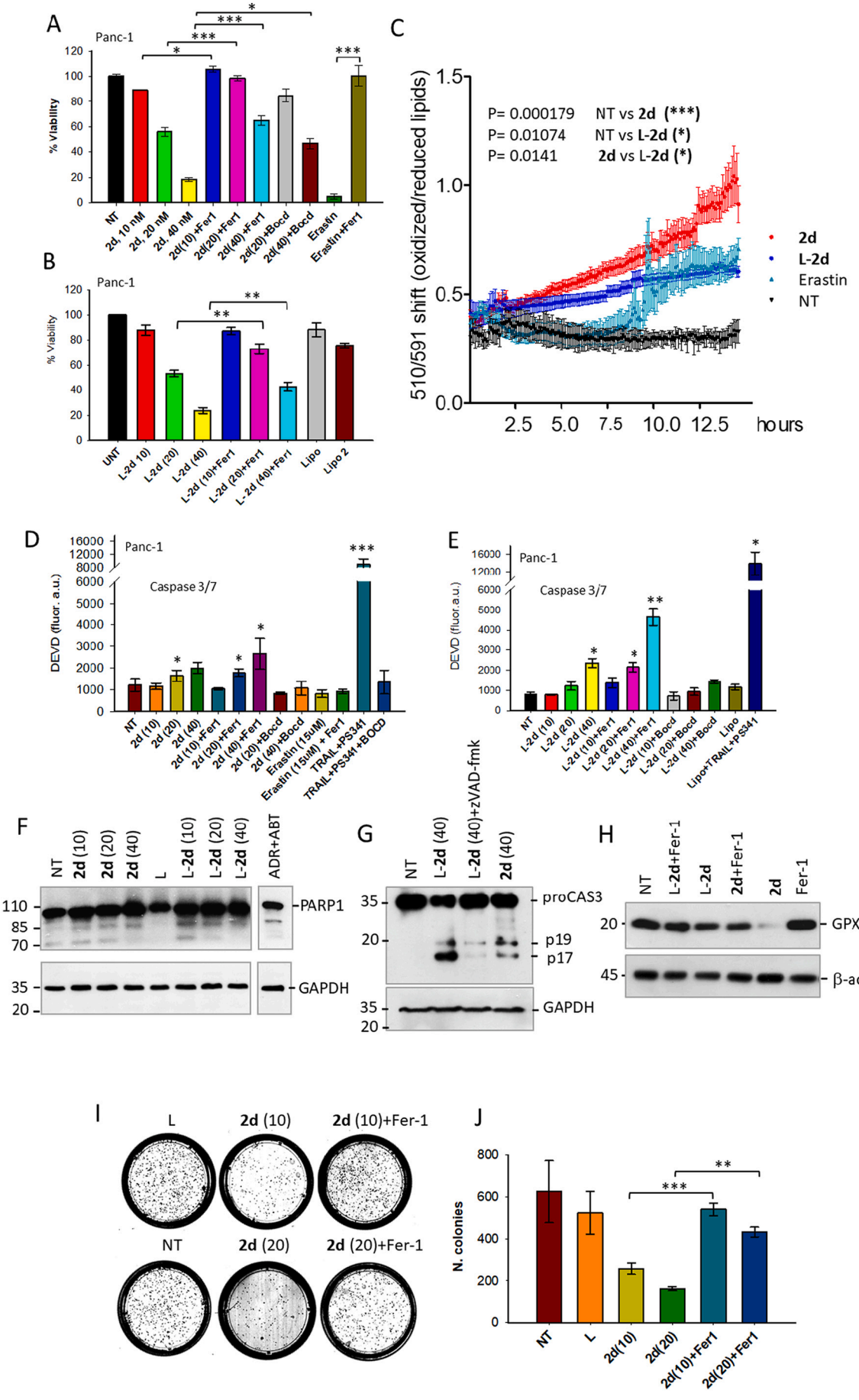

(caption on next page)

Fig. 7. (A) Cell viability assay (% compared to cells treated only with light). Panc-1 cells phototreated with **2d**, **2d** + Fer-1, **2d** + Bocd, erastin, erastin + Fer-1; (B) Viability assay of Panc-1 cells phototreated with L-**2d**, L-**2d** + Fer-1 and L (empty liposome); (C) Fluorescence ratio of C11-Bodipy $^{581/591}$ as a function of time for single cell loaded with the probe and **2d** or L-**2d**. The analysis was extended to a number of cells varying from 11 to 27 up to 15 h since illumination; (D, E) Caspase 3/7 activity assay. Panc-1 cells were phototreated with **2d**, **2d** + Fer-1, **2d** + Bocd, erastin, erastin + Fer-1, TRAIL+PS341, TRAIL+PS341 + bocd, L = liposome; (F, G) Western blots showing the expression of PARP-1, pro-caspase 3 and GAPDH in Panc-1 cells treated with **2d**, L-**2d**, ADR + ABT; (H) Expression of GPX4 and β-actin in Panc-1 cells treated with **2d**, Fer-1, **2d** + Fer-1, L-**2d**, L-**2d** + Fer-1. $P \leq 0.05$ (*), 0.01 (**), 0.001 (***); (I, J) Clonogenic assay of Panc-1 cells treated with liposome (L), **2d**, L-**2d**, **2d** + Fer-1. Bar plot reporting the number of colonies in untreated and treated Panc-1 cells 15 days after illumination. Each experiment has been performed in triplicate. P ≤ 0.05 (*), 0.01 (**), 0.001 (***).

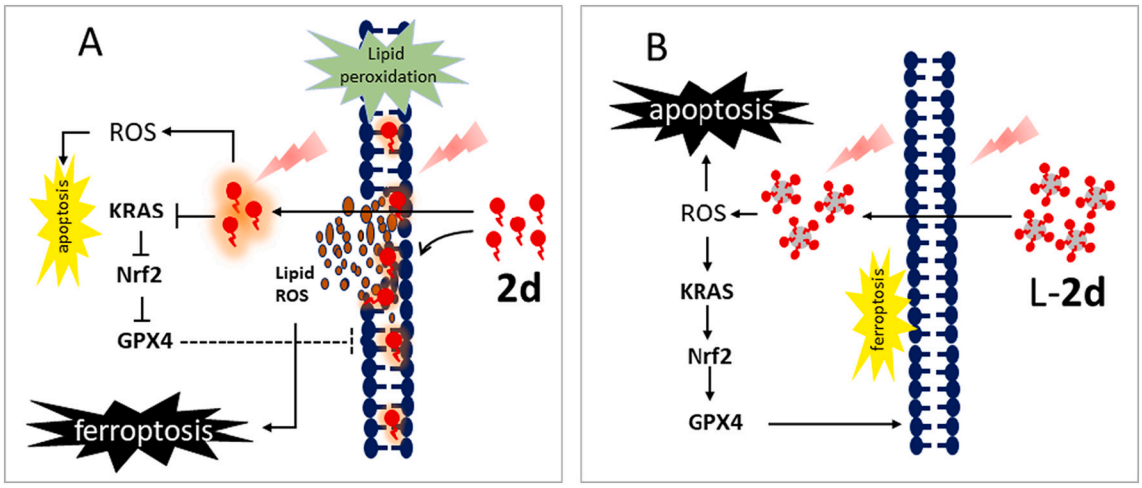

Fig. 8. (A, B) Putative mechanism of action of liposome-bound porphyrin (L-**2d**) and free porphyrin (**2d**). Free alkyl-porphyrin **2d** binds to the membrane and inhibits the *KRAS*-Nrf2-GPX4 axis. This results in lipid peroxidation and lipid ROS formation that trigger ferroptosis. In contrast, liposome-bound L-**2d** neither loads the membrane with **2d** molecules nor inhibits the *KRAS*-Nrf2-GPX4 axis. Upon illumination it generates ROS that promote a mechanism of cell death mainly based on apoptosis.

desigh of combination therapies.

Funding

This work was supported by AIRC (the Italian Association for Cancer Research). Grant number: IG 2017, Project Code 19898. Work at the Biomolecular Nanoscale Engineering Center (BioNEC), a Centre of Excellence has been funded by THE VILLUM FOUNDATION (grant no. VKR022710, S.V and P.M.G.L.). Funding for open access charge: AIRC (the Italian Association for Cancer Research).

CRediT authorship contribution statement

Eros Di: Giorgio Conceptualization, Investigation, Supervision. **Annalisa Ferino:** Investigation, Supervision. **Himanshi Choudhary:** Investigation. **Phillip M.G. Löffler:** Investigation, Resources. **Francesca D'Este:** Investigation. **Valentina Rapozzi:** Investigation. **Alexander Tikhomirov:** Resources, Formal analysis. **Andrey Shchekotikhin:** Resources, Formal analysis. **Stefan Vogel:** Resources, Formal analysis. **Luigi E. Xodo:** Conceptualization, Funding acquisition, Writing – original draft.

Declaration of Competing Interest

The authors declare that they have no known competing financial interests or personal relationships that could have appeared to influence the work reported in this paper.

Appendix A. Supplementary data

Supplementary data to this article can be found online at https://doi.org/10.1016/j.jphotobiol.2022.112449.

References

[1] G.A. Koning, G. Storm, Targeted drug delivery systems for the intracellular delivery of macromolecular drugs, Drug Discov. Today 8 (2003) 482–483, https://doi.org/10.1016/s1359-6446(03)02699-0.
[2] J.M. Metselaar, G. Storm, Liposomes in the treatment of inflammatory disorders, Expert. Opin. Drug Deliv. 2 (2005) 465–476, https://doi.org/10.1517/17425247.2. 3.465.
[3] B.S. Ding, T. Dziubla, V.V. Shuvaev, S. Muro, V.R. Muzykantov, Advanced drug delivery systems that target the vascular endothelium, Mol. Interv. 6 (2006) 98–112, https://doi.org/10.1124/mi.6.2.7.
[4] S. Hua, S.Y. Wu, The use of lipid-based nanocarriers for targeted pain therapies, Front. Pharmacol. 4 (2013) 143, https://doi.org/10.3389/fphar.2013.00143.
[5] D.R. Khan, E.M. Rezler, J. Lauer-Fields, G.B. Fields, Effects of drug hydrophobicity on liposomal stability, Chem. Biol. Drug Des. 71 (2008) 3–7, https://doi.org/10.1111/j.1747-0285.2007. 00610.x.
[6] T.M. Allen, P.R. Cullis, Liposomal drug delivery systems: from concept to clinical applications, Adv. Drug Deliv. Rev. 65 (2013) 36–48, https://doi.org/10.1016/j.addr.2012.09.037.
[7] B.S. Pattni, V.V. Chupin, V.P. Torchilin, New developments in liposomal drug delivery, Chem. Rev. 115 (2015) 10938–10966, https://doi.org/10.1021/acs.chemrev.5b00046.
[8] A. Akbarzadeh, et al., Liposome: classification, preparation, and applications, Nanoscale Res. Lett. 8 (2013) 102–111, https://doi.org/10.1186/1556-276X-8-102.
[9] N. Oku, K. Doi, Y. Namba, S. Okada, Herapeutic effect of adriamycin encapsulated in long-circulating liposomes on meth-A-sarcoma-bearing mice, Int. J. Cancer 58 (1994) 415–419, https://doi.org/10.1002/ijc.2910580318. 10.1002/ijc.2910580318.
[10] A.S. Ulrich, Biophysical aspects of using liposomes as delivery vehicles, Biosci. Rep. 22 (2002) 129–150, https://doi.org/10.1023/a:1020178304031.
[11] V.P. Torchilin, Liposomes as delivery agents for medical imaging, Mol Med Today. 2 (1996) 242–249, https://doi.org/10.1016/1357-4310(96)88805-8.
[12] Y. Liu, K.M. Castro Bravo, J. Liu, Targeted liposomal drug delivery: a nanoscience and biophysical perspective, J. Nanoscale Horiz. 6 (2021) 78–94, https://doi.org/10.1039/d0nh00605j.
[13] A. Ferino, G. Nicoletto, F. D'Este, S. Zorzet, S. Lago, S.N. Richter, A. Tikhomirov, A. Shchekotikhin, L.E. Xodo, Photodynamic therapy for *ras*-driven cancers: targeting G-Quadruplex RNA structures with bifunctional alkyl-modified porphyrins, J. Med. Chem. 63 (2020) 1245–1260, https://doi.org/10.1021/acs.jmedchem.9b01577.
[14] G. Miglietta, S. Cogoi, J. Marinello, G. Capranico, A.S. Tikhomirov, A. Shchekotikhin, L.E. Xodo, RNA G-Quadruplexes in Kirsten Ras (KRAS) oncogene

as targets for small molecules inhibiting translation, J. Med. Chem. 60 (2017) 9448–9461, https://doi.org/10.1021/acs.jmedchem.7b00622.
[15] S. Burge, G.N. Parkinson, P. Hazel, A.K. Todd, S. Neidle, Quadruplex DNA: sequence, topology and structure, Nucleic Acids Res. 34 (2006) 5402–5415, https://doi.org/10.1093/nar/gkl655.
[16] J. Spiegel, S. Adhikari, S. Balasubramanian, The structure and function of DNA G-Quadruplexes, Trends in Chemistry. 2 (2020) 123–136, https://doi.org/10.1016/j.trechm.2019.07.002.
[17] H. Ying, A.C. Kimmelman, C.A. Lyssiotis, S. Hua, G.C. Chu, E. Fletcher-Sananikone, J.W. Locasale, J. Son, H. Zhang, J.L. Coloff, et al., Oncogenic kras maintains pancreatic tumors through regulation of anabolic glucose metabolism, Cell 149 (2012) 656–670, https://doi.org/10.1016/j.cell.2012.01.058.
[18] J. Son, C.A. Lyssiotis, H. Ying, X. Wang, S. Hua, M. Ligorio, R.M. Perera, C. R. Ferrone, E. Mullarky, N. Shyh-Chang, et al., Glutamine supports pancreatic cancer growth through a KRAS-regulated metabolic pathway, Nature. 496 (2013) 101–105, https://doi.org/10.1038/nature12040.
[19] A. Ferino, V. Rapozzi, L.E. Xodo, The ROS-KRAS-Nrf2 axis in the control of the redox homeostasis and the intersection with survival-apoptosis pathways: implications for photodynamic therapy, J. Photochem. Photobiol. B 202 (2020), 111672, https://doi.org/10.1016/j.jphotobiol.2019.111672.
[20] S. Mukhopadhyay, D. Goswami, P.P. Adiseshaiah, W. Burgan, M. Yi, T.M. Guerin, S.V. Kozlov, D.V. Nissley, F. McCormick, Undermining Glutaminolysis bolsters chemotherapy while NRF2 promotes Chemoresistance in KRAS-driven pancreatic cancers, Cancer Res. 80 (2020) 1630–1643, https://doi.org/10.1158/0008-5472.CAN-19-1363.
[21] K. Susanne, Golombek, Jan-Niklas may, Benjamin Theek, Lia Appold, Natascha Drude, Fabian Kiessling, and Twan Lammers tumor targeting via EPR: strategies to enhance patient responses, Adv. Drug Deliv. Rev. 130 (2018) 17–38, https://doi.org/10.1016/j.addr.2018.07.007.
[22] M.K. Kuimova, G. Yahioglu, P.R. Ogilby, Singlet oxygen in a cell: spatially dependent lifetimes and quenching rate constants, J. Am. Chem. Soc. 14 (131) (2009) 332–340, https://doi.org/10.1021/ja807484b.
[23] U. Jakobsen, S. Vogel, Chapter 12 - DNA-controlled assembly of liposomes in diagnostics, Methods Enzymol. 464 (2009) 233–248, https://doi.org/10.1016/S0076-6879(09)64012-X.
[24] H.T. McMahon, E. Boucrot, Molecular mechanism and physiological functions of clathrin-mediated endocytosis, Nat Rev Mol Cell Biol. 12 (2011) 517–533, https://doi.org/10.1038/nrm3151.
[25] P. Davies, A.C. Allison, Effects of cytochalasin B on endocytosis and exocytosis, Front. Biol. 46 (1978) 143–160. 352738.
[26] E.L. Eskelinen, Roles of LAMP-1 and LAMP-2 in lysosome biogenesis and autophagy, Mol. Asp. Med. 27 (5–6) (2006) 495–502, https://doi.org/10.1016/j.mam.2006.08.005.
[27] Irina Raykhel, Heli Alanen, Kirsi Salo, Jaana Jurvansuu, Van Dat Nguyen, Maria Latva-Ranta, and Lloyd Ruddock. A molecular specificity code for the three mammalian KDEL receptors, J. Cell Biol. 179 (2007) 1193–1204, https://doi.org/10.1083/jcb.200705180.
[28] L. Castro, B.A. Freeman, Reactive oxygen species in human health and disease, Nutrition 2001 (161) (2001) 163–165, https://doi.org/10.1016/s0899-9007(00)00570-0.
[29] G.M. DeNicola, F.A. Karreth, T.J. Humpton, A. Gopinathan, C. Wei, et al., Oncogene-induced Nrf2 transcription promotes ROS detoxification and tumorigenesis, Nature 475 (2011) 106–109, https://doi.org/10.1038/nature10189.
[30] A. Lister, T. Nedjadi, N.R. Kitteringham, F. Campbell, E. Costello, et al., Nrf2 is overexpressed in pancreatic cancer: implications for cell proliferation and therapy, Mol. Cancer 10 (2011) 37, https://doi.org/10.1186/1476-4598-10-37.
[31] J.M. Matés, C. Pérez-Gòmez, I. Nùnez de Castro, Antioxidant enzymes and human diseases, Clin. Biochem. 32 (1999) 595–603, https://doi.org/10.1016/s0009-9120(99)00075-2.
[32] Q. Ma, Role of Nrf2 in oxidative stress and toxicity, Annu. Rev. Pharmacol. Toxicol. 53 (2013) 401–426, https://doi.org/10.1146/annurev-pharmtox-011112-140320.
[33] G. Cinque, A. Ferino, E.B. Pedersen, L.E. Xodo, Role of poly [ADP-ribose] polymerase 1 in activating the *Kirsten ras* (*KRAS*) gene in response to oxidative stress, Int. J. Mol. Sci. 21 (2020) 6237, https://doi.org/10.3390/ijms21176237.
[34] M. da Silva Baptista, J. Cadet, P. Paolo Di Mascio, A.A. Ghogare, A. Greer, et al., Type I and II photosensitized oxidation reactions: guidelines and mechanistic Pathways, Photochem. Photobiol. 93 (2017) 912–919, https://doi.org/10.1111/php.12716.
[35] S. Eser, A. Schnieke, G. Schneider, D. Saur, Oncogenic KRAS signalling in pancreatic cancer, Br. J. Cancer 111 (2014) 817–822, https://doi.org/10.1038/bjc.2014.215.
[36] S. Eser, N. Reiff, M. Messer, B. Seidler, K. Gottschalk, Selective requirement of PI3K/PDK1 signaling for Kras oncogene-driven pancreatic cell plasticity and cancer, Cancer Cell 23 (2013) 406–420, https://doi.org/10.1016/j.ccr.2013.01.023.
[37] R. Ferro, M. Falasca, Emerging role of the KRAS-PDK1 axis in pancreatic cancer, World J. Gastroenterol. 20 (2014) 10752–10757, https://doi.org/10.3748/wjg.v20.i31.10752.
[38] K.M. Holmstrom, T. Finkel, Cellular mechanisms and physiological consequencesof redox-dependent signalling, Nat. Rev. Mol. Cell Biol. 15 (2014) 411–421, https://doi.org/10.1038/nrm3801.
[39] B. D'Autreaux, M.B. Toledano, ROS as signalling molecules: mechanisms that generate specificity in ROS homeostasis, Nat. Rev. Mol. Cell Biol. 8 (2007) 813–824, https://doi.org/10.1038/nrm2256.
[40] C. Wen, H. Wang, X. Wu, et al., ROS-mediated inactivation of the PI3K/AKT pathway is involved in the antigastric cancer effects of thioredoxin reductase-1 inhibitor chaetocin, Cell Death Dis. 10 (2019) 809, https://doi.org/10.1038/s41419-019-2035-x.
[41] J. Cao, D. Xu, D. Wang, R. Wu, L. Zhang, ROS-driven Akt dephosphorylation at Ser-473 is involved in 4-HPR-mediated apoptosis in NB4 cells, Free Radic. Biol. Med. 47 (2009) 536–547, https://doi.org/10.1016/j.freeradbiomed.2009.05.024.
[42] Y. Son, Y.-K. Cheong, N.-K. Kim, H.-T. Chung, D.G. Kang, H.-O. Pae, Mitogen-Activated Protein Kinases and Reactive Oxygen Species: How Can ROS Activate MAPK Pathways? J. Signal. Trans. (2011), 792639 https://doi.org/10.1155/2011/792639.
[43] S.J. Dixon, K.M. Lemberg, M.R. Lamprecht, R. Skouta, E.M. Zaitsev, et al., Ferroptosis: an iron-dependent form of nonapoptotic cell death, Cell 149 (2012) 1060–1072, https://doi.org/10.1016/j.cell.2012.03.042.
[44] W.S. Yang, B.R. Stockwell, Synthetic lethal screening identifies compounds activating iron-dependent, nonapoptotic cell death in oncogenic-RAS-harboring cancer cells, Chem. Biol. 15 (2008) 234–245, https://doi.org/10.1016/j.chembiol.2008.02.010.
[45] L. Yang, X. Chen, Q. Yang, J. Chen, Q. Huang, Front. Oncol. 10 (2020) 949, https://doi.org/10.3389/fonc.2020.00949.
[46] S. Dolma, S.L. Lessnick, W.C. Hahn, B.R. Stockwell, Identification of genotype-selective antitumor agents using synthetic lethal chemical screening in engineered human tumor cells, Cancer Cell 3 (2003) 285–296, https://doi.org/10.1016/s1535-6108(03)00050-3.
[47] R. Skouta, S.J. Dixon, J. Wang, D.E. Dunn, M. Orman, et al., Ferrostatins inhibit oxidative lipid damage and cell death in diverse disease models, J. Am. Chem. Soc. 136 (2014) 4551–4556, https://doi.org/10.1021/ja411006a.
[48] L. Cao, Y. Liang, Y. Liu, Y. Xu, W. Wan, C. Zhu, Pseudo-phosphorylation at AT8 epitopes regulates the tau truncation AT aspartate 421, Exp. Cell Res. 370 (2018) 103, https://doi.org/10.1016/j.yexcr.2018.06.010.
[49] J. Li, J. Li, Y. Pu, S. Li, W. Gao, B. He, PDT-enhanced Ferroptosis by a polymer nanoparticle with pH-activated singlet Oxygen generation and superb biocompatibility for Cancer therapy, Biomacromolecules 22 (2021) 1167, https://doi.org/10.1021/acs.biomac. 0c01679.
[50] E.H. Pap, G.P.C. Drummen, V.J. Winter, T.W.A. Kooij, P.J. Rijken, Ratio-fluorescence microscopy of lipid peroxidation in living cells using C11-BODIPY581/591, FEBS Lett. 453 (1999) 278–282, https://doi.org/10.1016/s0014-5793(99)00696-1.
[51] G.P.C. Drummen, L.C. Mvan, L.C.M. van Liebergen, J. Op den Kamp, J.A. Post, C11-BODIPY$^{581/591}$, an oxidation-sensitive fluorescent lipid peroxidation probe: (micro)spectroscopic characterization and validation of methodology, Free Radic. Biol. Med. 33 (2002) 473–490, https://doi.org/10.1016/s0891-5849(02)00848-1.
[52] G.C. Forcina, S.J. Dixon, GPX4 at the crossroads of lipid homeostasis and Ferroptosis, Proteomics 19 (2019), e1800311, https://doi.org/10.1002/pmic.201800311.
[53] C. Xu, S. Sun, T. Johnson, R. Qi, S. Zhang, J. Zhang, K. Yang, The glutathione peroxidase Gpx4 prevents lipid peroxidation and ferroptosis to sustain Treg cell activation and suppression of antitumor immunity, Cell Rep. 35 (2021), 109235, https://doi.org/10.1016/j.celrep.2021.109235.
[54] W. Liu, Y. Zhou, W. Duan, J. Song, S. Wei, et al., Glutathione peroxidase 4-dependent glutathione high-consumption drives acquired platinum chemoresistance in lung cancer-derived brain metastasis, Clin. Transl. Med. 11 (2021), e517, https://doi.org/10.1002/ctm2.517.